Tracer dispersion in three-dimensional multipole flows

Ming Zhang and Joel Koplik
Benjamin Levich Institute and Department of Physics, City College of the City University of New York, New York, New York 10031
(Received 23 January 1997)

The transit time distribution for the hydrodynamic dispersion of a passive tracer in three-dimensional reservoir configurations of localized sources and sinks is related to the large-scale geometry of the system. Extending previous work on the planar case, we find that the first-passage transit time probability distribution function has a region of power-law decay, depending only on the multipole order of the distribution of fluid sources and sinks, an exponential decay region, whose characteristics are related to stagnation points in the flow field, and a shoulder whose location is related to the system size. Tracer measurements may thus be used as a noninvasive surface diagnostic tool to characterize subsurface reservoirs. [S1063-651X(97)11710-X]

PACS number(s): 47.55.Mh, 05.40.+j

I. INTRODUCTION

The majority of theoretical and laboratory studies of hydrodynamic dispersion in porous media focus on flows in which the average fluid and tracer motion is one dimensional [1–5]. Aside from the relative ease of analysis associated with quasi-one-dimensional behavior, this configuration arises automatically in studies of cylindrical ''cores'' of natural porous material extracted during drilling. However, in many practical applications to aquifers and hydrocarbon reservoirs, fluid enters and leaves the system through wells, which are localized sources in three dimensions, and so the flow is *multipolar* rather than linear on average. Three previous papers [6–8] (referred to henceforth as I, II, and III, respectively) considered dispersion in multipole flow in two dimensions, appropriate to an approximately planar porous stratum in the earth. The results indicated first that dispersion in two-dimensional (2D) multipole flow differed qualitatively from the quasilinear case, and second that the distribution of transit times between sources and sinks incorporates a great deal of information about the reservoir geometry. This paper extends the earlier methodology to the more general case of 3D systems, and we find a qualitative similarity but important quantitative differences.

We will consider a steady incompressible fluid flow in a three-dimensional porous medium, satisfying Darcy's law, into which a δ-function pulse of passive tracer is inserted at time $t=0$. The flux of tracer exiting the system as a function of time, $p(t)$, will be the focus of the analysis. Typically, in petroleum recovery applications, for example, fluid enters the medium at an injection well and exits at one or more producing wells, and the well diameters are very small compared to the extent of the reservoir. In consequence there is effectively a point source and multiple point sinks for fluid, and the flow field is a potential flow *multipole*. The tracer concentration $c(\vec{r},t)$ is assumed to satisfy an appropriate local convective diffusion equation with boundary conditions corresponding to unit source of flux, reflecting conditions at the boundaries of the porous medium, and absorbing boundary conditions corresponding to point sinks at the flow outlet(s). (The fluid velocity at entry and exit is large in practice, and tracer backflow is negligible.) An equivalent problem is that of a random walker who starts at the inlet, executes a walk whose random steps are biased by the local velocity field, and is absorbed at the outlet; $p(t)$ is then identical to the first-passage probability distribution function for arrival at the sink.

The mathematical problem is formulated as follows. The potential flow due to a set of sources and sinks at positions $\{\vec{a}_i\}$ with respective volumetric fluxes $\{Q_i\}$ is

$$\vec{u}(\vec{r})=\vec{\nabla}\Phi(\vec{r}),$$

where

$$\Phi=-\sum_i \frac{Q_i}{4\pi}\left[\frac{1}{|\vec{r}-\vec{a}_i|}+\frac{r}{a_i|\vec{r}-\vec{A}_i|}\right], \tag{1}$$

where Φ is the velocity potential, proportional to the fluid pressure, and it is assumed that we have a closed system so that $\Sigma_i Q_i=0$. In most cases we are interested in a finite spatial region with impermeable boundaries, which we take to be a sphere of radius R, on which the normal fluid velocity should vanish. The terms in Eq. (1) involving $\vec{A}_i\equiv(R/a_i)^2\vec{a}_i$ are precisely the image sources [9] outside the sphere which enforce the latter condition. The tracer concentration $c(\vec{r},t)$ satisfies the convective diffusion equation (CDE)

$$\frac{\partial c}{\partial t}+\vec{u}(\vec{r})\cdot\vec{\nabla}c=D\nabla^2 c, \tag{2}$$

with diffusivity D. Strictly speaking one should use the effective diffusivity tensor [1–5] which is a function of the velocity $\vec{u}(\vec{r})$, but as shown in II, the results for multipole flows are independent of which is used. The reason is that the modifications to D are only important when the local Péclet number is large, but in this case the tracer motion is

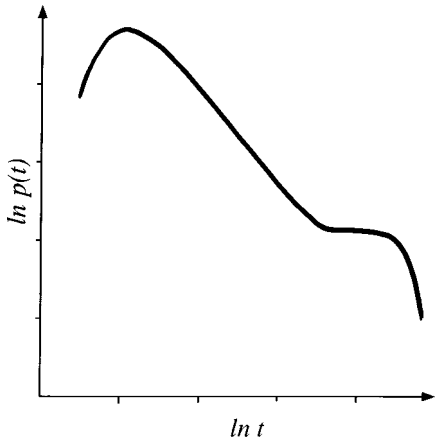

FIG. 1. Generic form of the transit time distribution obtained in this paper.

dominated by convection anyway, while at low Péclet numbers where diffusion matters, the corrections are unimportant to the scaling behavior.

The distinction between the well-studied case of core flows and the higher-dimensional flows considered here is that in the former case the velocity field is constant on average, so that a tracer pulse simply translates with the mean velocity and spreads about its center due to (convectively enhanced) diffusion. All fluid streamlines run more or less unidirectionally from source to sink and, at least in the statistically homogeneous and isotropic case, are affected by the same random environment. There is thus a well-defined mean velocity about which the individual tracer particles fluctuate, so that the tracer exit profile is sigmoidal. The most interesting feature is the width of the step, which can be related to the effective tracer diffusivity, and large-scale heterogeneities manifest themselves as long-time tails in $p(t)$. In higher dimensions, the flow is instead multipolar and spreads the tracer in all directions. Since the velocity is a strongly varying function of position, different packets of tracer are affected by entirely different environments.

A qualitative analysis of the features of the transit time distribution in the multipole case is as follows. The flow field can be divided into several subregions, which are in one-to-one correspondence with distinct features in a typical plot of $p(t)$ vs time given in Fig. 1. (1) The early arrival regime corresponds to tracer which moves roughly directly from source to sink. This part of the curve is sensitive to small-scale features of the geometry, such as the distance from source to sink, and will not be considered in detail here. Tracer which does not initially head towards the sink is carried out into the porous medium on a streamline of the multipole flow field. (2) Those streamlines which simply circle between source and sink without approaching the system boundaries are scale invariant—the velocity decays as a power of distance and, as we shall discuss, there is a corresponding power-law decay in $p(t)$. (3) Some outgoing streamlines do pass near the boundary of the medium and are distorted from a pure multipole form; tracer particles following such streamlines in a sense reflect from the boundary, and produce an enhancement or bump in $p(t)$ above the value associated with pure multipole flow. This ''echo'' effect occurs at a time given by the transit time from source to boundary to sink. Since velocities tend to be small near the boundary, the local Péclet number is often small there, and the tracer motion and the corresponding transit time would be diffusive. (4) Outgoing streamlines which approach a stagnation point have velocities which vary linearly with the distance from it. Correspondingly, tracer particles following such streamlines spend an exponentially long time near the stagnation point, leading (see below) to an exponential decay in $p(t)$. (5) If the system is large enough, and/or the fluid velocity is small enough, the motion will be predominantly diffusive at large distances from the sources and sinks. In this case the tail of $p(t)$ is controlled by simple diffusion in a finite region, and an exponential decay is expected. In drawing the figure, we have omitted the distinction between regions (4) and (5), but it was observed in some of the 2D cases in II.

The general arguments in the last paragraph summarize the 2D results in [6–8] and their demonstration in 3D will be the subject of this paper. In addition, the detailed arguments to follow will provide universal numerical values for the power-law exponents, and system-dependent estimates for the exponential decay rates. The methods used here directly extend those of the earlier papers to 3D, and we proceed in a similar fashion. In Sec. II we focus on the power-law regime, and consider the limit of pure convection in multipole flows. To incorporate diffusion, but remain at high Péclet numbers, a numerical method based on individual random walkers is optimal. At low Péclet number it is more efficient to consider the ensemble of random walkers, or equivalently the continuum CDE. We discuss and implement two related methods, which may be described as ''probability propagation.'' These methods are reviewed and applied in Sec. III. Lastly we turn in Sec. IV to the effects of systematic deviations from statistical homogeneity in the porous medium. For weakly correlated fluctuations we find no change in our results until the magnitude of the relative perturbation is $O(1)$. Large-scale heterogeneities, such as impermeable barriers, do yield significant changes, however, and we discuss one nontrivial example in detail. A summary and conclusions appear in Sec. VII. A very general argument for the power-law exponents, due to Hinch [10], is given in the Appendix.

II. PURE CONVECTION

Most of the behavior we find in multipole flows appears in the limit of pure convection, or infinite Péclet number, and furthermore analytic arguments are possible in this case. We first consider simple dipole flows numerically, then relate the observed features to simple approximate analytic calculations, and finally verify the systematic behavior in more complicated configurations.

A. Simple dipole flow

In pure convection tracer particles are simply carried along their initial streamlines, so that the CDE is replaced by

$$\frac{d\vec{r}(t)}{dt}=\vec{u}(\vec{r}(t)). \tag{3}$$

The velocity $\vec{u}(\vec{r})$ is given by Eq. (2), specialized to the case of a source and sink placed at $a_{1,2}=(0,0,\mp a)$, respectively. We nondimensionalize all lengths using a, and time using $4\pi a^3/Q$, so that the equations of motion simplify to $\vec{u}(\vec{r})=\vec{\nabla}\Phi$ with

$$\Phi=[V_1(0,0,-1)+rV_1(0,0,-R^2)] +[V_1(0,0,+1)+rV_1(0,0,+R^2)], \quad (4)$$

where $V_1(\vec{r}_0)\equiv -1/|\vec{r}-\vec{r}_0|$ is the potential of a point source at $\vec{r}_0$. The terms in Eq. (4) are the source and sink at $(0,0,\mp 1)$ along with the image sources at $(0,0,\mp R^2)$ which are needed to make the normal velocity $\hat{r}\cdot\vec{\nabla}\Phi$ vanish on a sphere of radius R [9]. The flow is symmetric about the z axis and convective tracer motion is confined to a plane of constant azimuthal angle ϕ.

If the flow domain is unbounded, corresponding to $R\to\infty$ in Eq. (4), we can actually find the transit time distribution analytically. In II it was shown for planar convection in a simple dipole velocity field that the transit time from source to sink along a streamline is

$$t(\theta)=2\csc^2\theta[1-\theta\cot\theta]\underset{\theta\to\pi}{\to}\frac{2\pi}{(\pi-\theta)^3}. \quad (5)$$

Here θ is the initial angle with respect to the dipole axis, with the convention that $\theta=0(\pi)$ is the direction towards (away from) the sink. Convective motion in a static flow field is deterministic, but a probability distribution of transit times results from a distribution of initial angles θ:

$$p(t)=p(\theta)\left|\frac{d\theta}{dt}\right|. \quad (6)$$

The initial angle distribution is determined by the physical consideration that tracer emitted from a high-velocity point source will spread out uniformly in direction, corresponding to the locally radial velocity profile $\vec{u}(\vec{r})\approx\vec{\nabla}V_1(0,0,-1)$. The appropriate distribution of initial angle is then $p(\theta)\propto\sin\theta$, uniform in solid angle. Substituting into Eq. (6) we obtain $p(t)\sim t^{-5/4}$. A simple and self-contained but approximate argument for this result will be given below. [In the completely planar case considered in II, $p(\theta)$ is a constant and $p(t)\sim t^{-4/3}$.]

If we return to a spherical flow domain and retain the image terms, the transit time distribution must be found numerically. A random initial angle is chosen with probability distribution $p(\theta)$, Eq. (3) is integrated numerically (using a variable-step, variable-order, backwards difference routine), and $p(t)$ is found numerically from Eq. (6). The result is shown in a log-log plot in Fig. 2(a): there is a seven-decade region of times where $p(t)\sim t^{-5/4}$, followed by a cutoff. (The early-time regime is omitted as being uninteresting.) As in II, streamlines with initial angles near but not too near to π are not distorted by the impermeable boundaries, and the infinite-space analytic result should and does apply. For θ very close to π the streamlines approach stagnation points on the boundary of the confining sphere at $\vec{r}=(0,0,\mp R)$, and the tracer motion is substantially altered. In Fig. 2(b), we show the long-time region in a semilog plot, which is well fit by $p(t)\sim e^{-t/\tau}$ with $\tau=2.5\times 10^7$.

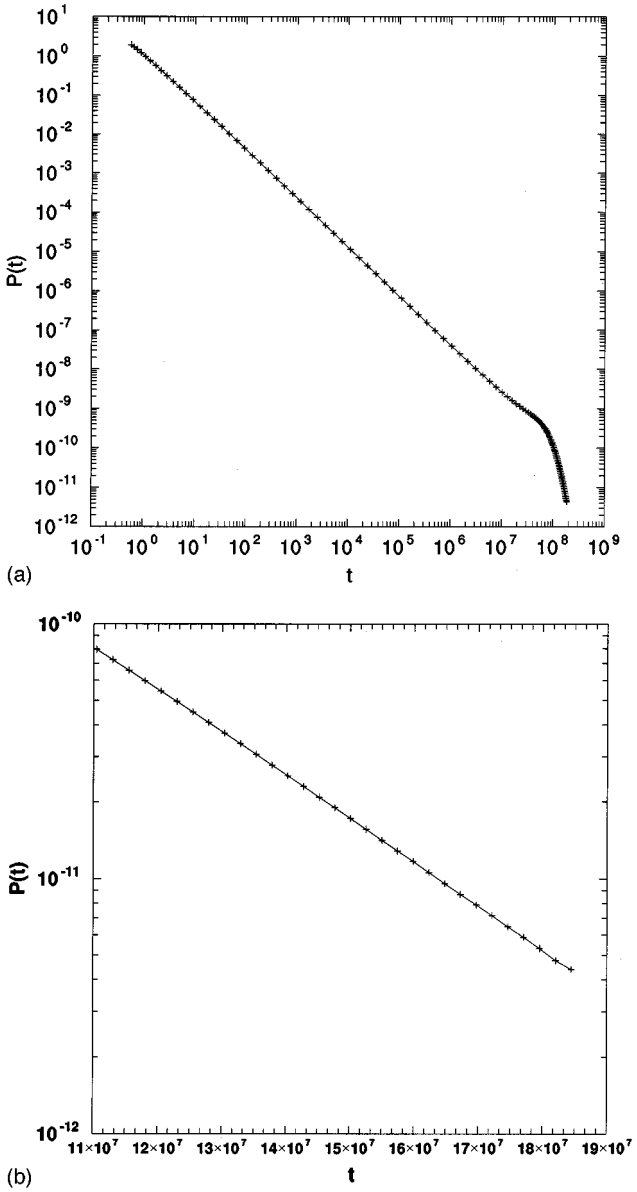

FIG. 2. Transit time distribution for pure convection for a simple source-sink dipole inside a sphere; (a) complete range of times, (b) tail region.

Because the motion is planar, the decay constant τ may be found directly using previous arguments for the 2D case. It was shown in II that the distribution of transit times $P(T)$ for particles to traverse the region near a 2D stagnation point is

$$P(T)=P_0(x_0)\left|\frac{dx_0}{dT}\right|\underset{x_0\to 0}{\sim}P_0(0)e^{-GT}. \quad (7)$$

In this expression, x_0 is the initial displacement transverse to the streamline leading to the stagnation point, with probability distribution P_0, and $G \equiv |\partial u_z/\partial z|$, where z is the local coordinate along the streamline. The trajectories leading to the tail region of $p(t)$ have relatively large velocities near the source and sink, exponentially small velocities near the two antipodal stagnation points, and $O(R^{-3})$ velocities on the circular arc near the sphere boundary. The overall transit time is dominated by the two stagnation regions, so $t \approx 2T$ and $p(t) \approx P_0(t=2T) \sim e^{-(G/2)t}$ where

$$G = \left| \frac{8(R^2+1)^2}{R^2(R^2-1)^3} \right| \tag{8}$$

is the derivative of the velocity field arising from Eq. (4). Substituting $R=100$, we obtain $\tau = 2.5 \times 10^7$, in agreement with the numerical results. The extension of this result to fully 3D trajectories will be given below in Sec. II D.

B. Power-law behavior

The power-law regime in $p(t)$ may be understood in terms of the general characteristics of motion along dipolar streamlines, as in I and II. We will consider the slightly more general case of tracer emission in an axially symmetric multipole flow, since the argument is essentially the same as for the dipole case. If in potential flow we have an arbitrary distribution of sources and sinks, $\rho(\vec{r})$, it is often useful to represent the solution as a multipole expansion

$$\Phi(\vec{r}) = -\sum_{l=0}^{\infty} \sum_{m=-l}^{l} \frac{4\pi}{2l+1} q_{l,m} r^{-l-1} Y_{l,m}(\theta,\phi), \tag{9}$$

where the $Y_{l,m}$ are spherical harmonics and $q_{l,m} = \int d^3 r r^{\prime l} Y_{lm}^*(\theta,\phi)\rho(\vec{r})$ are multipole moments. Suppose that far from the sources and sinks, and also far from the spherical boundary of the flow domain, the leading nonvanishing term in the distribution ρ is axially symmetric ($m=0$) and has multipole order n, so that

$$\Phi \sim r^{-n-1} P_n(\theta), \tag{10}$$

where P_n is a Legendre polynomial. For an incompressible axisymmetric flow, the velocity field may be given equivalently in terms of either the potential Φ or the stream function Ψ as

$$\vec{u}(\vec{r}) = (u_r, u_\theta) = \left(\frac{\partial \Phi}{\partial r}, \frac{1}{r}\frac{\partial \Phi}{\partial \theta} \right) = \left(\frac{-1}{r^2 \sin\theta}\frac{\partial \Psi}{\partial \theta}, \frac{1}{r\sin\theta}\frac{\partial \Psi}{\partial r} \right) \tag{11}$$

so from the asymptotic form of Φ we deduce

$$\Psi \sim \frac{\sin^2\theta P_n'(\cos\theta)}{n r^n}. \tag{12}$$

In the convective limit, a tracer particle remains on a streamline, where Ψ is a constant, so the trajectory is $r \sim (\sin^2\theta P_n\prime/n\Psi)^{1/n}$. Writing $u_\theta = r\dot{\theta}$, and eliminating r, we have $\dot{\theta} \sim f(\theta)\Psi^{(n+3)/n}$, where the explicit form of f will not be needed. Now for an nth-order multipole, the flow field consists of n lobes of roughly concentric streamlines, each of which traverses a certain range of θ. The transit time is then the time required for θ to run through the appropriate interval, and may be computed as

$$t = \int dt = \int_{\theta_1}^{\theta_2} \frac{d\theta}{\dot{\theta}} \sim \Psi^{-(n+3)/n}. \tag{13}$$

Next we must relate the value of Ψ to the angle at which a tracer particle is emitted from the source. The trajectories contributing to the tail of $p(t)$ are those which leave the source near $\theta = \pi$. If for $r = r_0$, $\theta = \pi - \epsilon$ with $r_0, \epsilon \ll 1$, then $\Psi \sim \epsilon^2$ from Eq. (8). The transit time distribution follows from Eq. (6), with $p(\theta) \sim \sin\theta \sim \epsilon$ and $t \sim \epsilon^{-2(n+3)/n}$:

$$p(t) \sim t^{-(2n+3)/(n+3)}. \tag{14}$$

For the dipole case of $n=1$, we recover $p(t) \sim t^{-5/4}$ as observed numerically.

C. Numerical results for other flows

We have actually studied a number of convective cases involving higher multipole moments [11], but the trend can be seen clearly from two further cases, an asymmetric flow to explore the effects of variation in azimuthal angle, and a higher multipole flow to verify the predicted variation with n.

First we consider an asymmetric dipole flow, arising from a source of (dimensionless) strength $+2$ at (0,0,1) and two sinks of strength -1 at $(0,\pm 1,0)$. The velocity potential, including image terms, is

$$\Phi(\vec{r}) = [2V_1(0,0,1) - V_1(0,1,0) - V_1(0,-1,0)] + r[2V_1(0,0,R^2) - V_1(0,R^2,0) - V_1(0,-R^2,0)]. \tag{15}$$

The planar streamlines in the y-z plane are shown in Fig. 3 for orientation, but the flow field generally varies with azimuthal angle ϕ. Figure 4 shows the numerical results: for the initial angle of emission of the tracer particle from the source we choose a value of ϕ and a range of θ near 0, and obtain $p(t)$ using the procedure described above. The curves resemble each other and, as summarized in Table I, both the power-law index and the exponential decay rate are independent of ϕ. The value of $n \approx 5/4$ is the same as for a symmetric dipole, while $\tau \approx 2.4 \times 10^7$ are close to each other but differ from the previous value for a simple dipole.

Secondly, we have studied a quadrupole ''five-spot'' pattern, often used in petroleum recovery, with a source of strength $+4$ at the origin and sinks of strength -1 at the

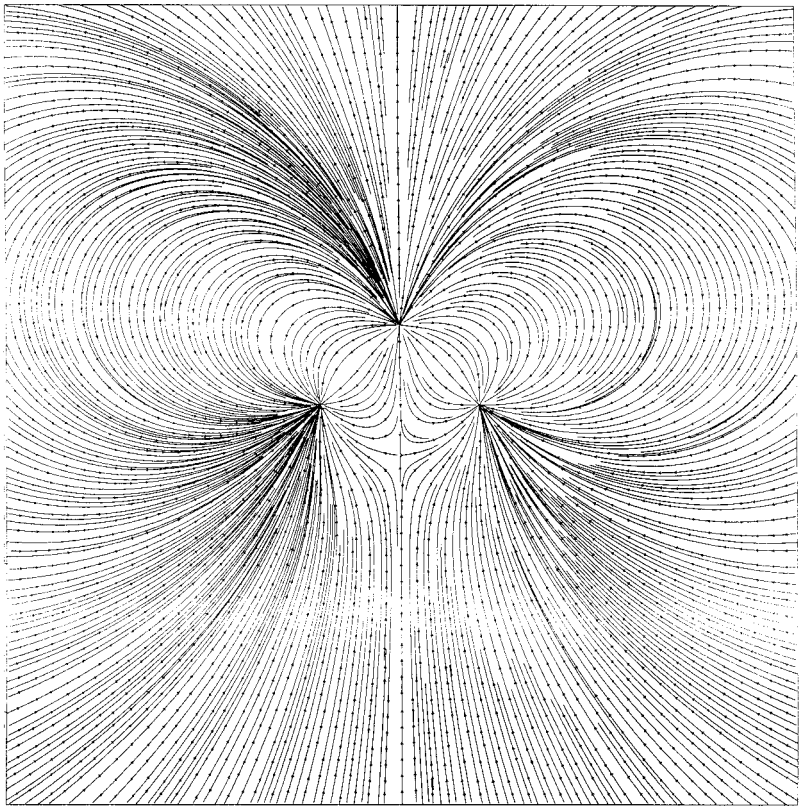

FIG. 3. Illustrative streamlines in the y-z plane for asymmetric dipole flow.

corners of a square in the x-y plane at (1,1,0), (1,−1,0), (−1,1,0), and (−1,−1,0). (In practice, the five spot is replicated roughly periodically.) Again we display the streamlines in the plane for orientation, in Fig. 3, and repeat the procedure of emitting tracer at various ϕ and a range of θ. The results shown in Fig. 5 and Table II show a power-law region with $p(t)\sim t^{-7/5}$ and an exponential decay tail with $\tau\approx 2.5\times 10^5$, both independent of the initial ϕ. The power-law exponent agrees with the theoretical estimate (10) with $n=2$, although the curves have a larger preasymptotic regime associated with the fact that the lobes of the quadrupole field are less developed.

The fact that the behavior of $p(t)$ is independent of the initial azimuthal angle ϕ came as a welcome surprise to us, since it permits an understanding of the results by analytic arguments. Subsequent to the original submission of this paper, an elegant and very general argument was found by Hinch, which is given in the Appendix.

D. Three-dimensional stagnation points

We wish to extend the 2D connection between stagnation points and exponential decay of $p(t)$ derived in II to the 3D case. Suppose the stagnation point lies at the origin, and expand the velocity potential locally as

$$\Phi(\vec{x})=a_0+\sum_i a_i x_i+\sum_{i,j} a_{i,j}x_i x_j+\cdots. \tag{16}$$

The constant a_0 is irrelevant, and the linear term vanishes identically if $\vec{x}=\vec{0}$ is a stagnation point. The matrix of quadratic coefficients $\{a_{i,j}\}$ is symmetric and can be diagonalized by a similarity transformation, and furthermore Laplace's equation implies that its trace is zero. Suppose that in the transformed coordinate system, $a_{11}<0$ so that a convected tracer particle approaching the origin along the 1-axis has $\dot{x}_1=-2|a_{11}|x_1$ and approaches the origin exponentially slowly, $x_1(t)=x_{10}e^{-2|a_{11}|t}$. In at least one of the other two directions, the corresponding diagonal quadratic term in Φ is positive, so, for example, $x_2(t)=x_{20}e^{+2a_{22}t}$ with $a_{22}>0$. A trajectory near the 1-axis approaching the origin will eventually diverge outwards from the stagnation point in the 2-direction. We can define a transit time T for the stagnation point region by requiring that the outgoing velocity is $O(1)$: $\dot{x}_2(T)=U_0=O(1)$. This definition yields $T=(2a_{22})^{-1}\ln U_0/2a_{22}x_{20}$. If the third diagonal element of Φ is negative, that coordinate tends to zero, while if it is positive the above argument should make use of the larger of a_{22} and a_{33} and its spatial direction.

The distribution of initial coordinates near the stagnation point leads to an exponential distribution of transit times:

$$P(T)=\int dx_{20}dx_{30}p(x_{20},x_{30})\delta\left(T-\frac{1}{2a_{22}}\ln\frac{U_0}{2a_{22}x_{20}}\right)$$

$$=U_0e^{-2a_{22}T}\int dx_{30}p\left(\frac{U_0}{2a_{22}}e^{-2a_{22}T},x_{30}\right)\underset{T\to\infty}{\sim} e^{-2a_{22}T}. \tag{17}$$

For the asymmetric dipole example with stagnation points at $(0,0,\mp R)$ one finds after some straightforward algebra that

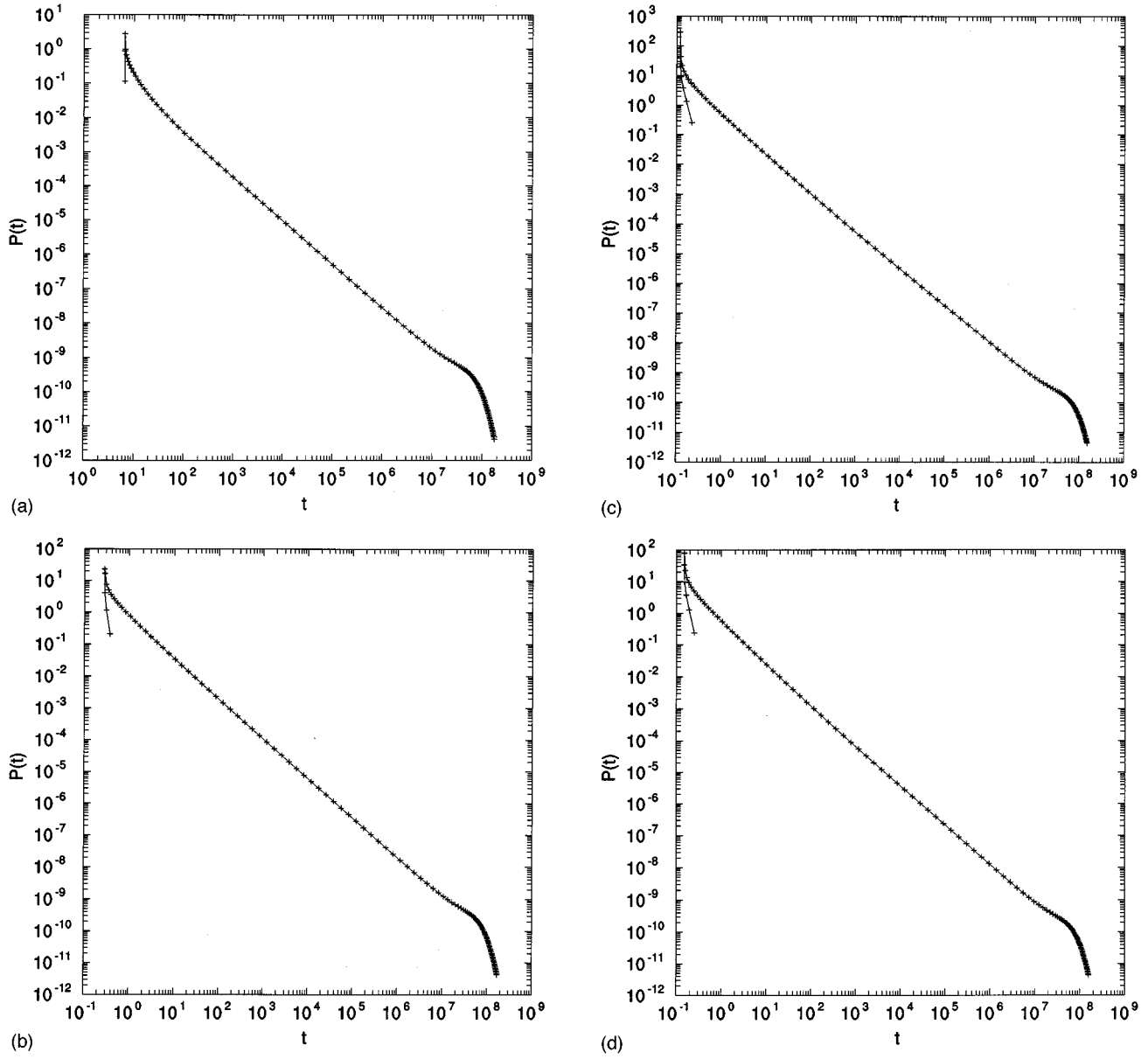

FIG. 4. Transit time distribution for pure convection in asymmetric dipole flow for various initial azimuthal angles; $\phi =$ (a) 0, (b) $\pi/6$, (c) $\pi/2$, (d) $2\pi/3$.

$\{a_{i,j}\}$ is diagonal with elements $a_{11}^{-1} = -4.9\times 10^5 \approx a_{22}^{-1}$ and $a_{33}^{-1} = 2.41\times 10^7$, where we have taken $R = 100$ as in the numerical simulations. The decay constant associated with the complete trajectory with two stagnation points is then twice $2a_{33}^{-1}$ or $\tau = 2.41\times 10^7$, in agreement with the numerical results, taking into account the uncertainty in estimating the decay constant from the numerical data. Similarly for the five-spot quadrupole flow, one finds $\tau = 2.50\times 10^{-5}$ analytically, in comparable agreement with the numerical values.

TABLE I. Power-law exponents $[p(t)\sim t^{-\alpha}]$ and exponential decay constants $[p(t)\sim e^{t/\tau}]$ fit to the numerical results for axisymmetric dipole flow, for various initial azimuthal angles.

ϕ_0	α	$\tau\times 10^{-7}$
0+	1.25±0.02	2.47±0.04
$\pi/6$	1.25±0.01	2.41±0.04
$\pi/3$	1.24±0.01	2.45±0.01
$\pi/2$	1.24±0.02	2.37±0.03
$2\pi/3$	1.25±0.01	2.41±0.01
$5\pi/6$	1.24±0.02	2.45±0.04
$\pi-$	1.25±0.02	2.47±0.04

III. INCORPORATION OF DIFFUSION

At any finite Péclet number tracer particles will of course diffuse as well as convect, but if Pe is large it is computationally convenient to simply add some random diffusive motion to the pure convection treated above [12]. Specifically, if a tracer particle is at $\vec{x}$ at time t, we adopt the displacement rule

$$\Delta\vec{x} = \vec{u}(\vec{x})\Delta t + \hat{n}\left(\frac{6\Delta t}{\mathrm{Pe}}\right)^{1/2}, \tag{18}$$

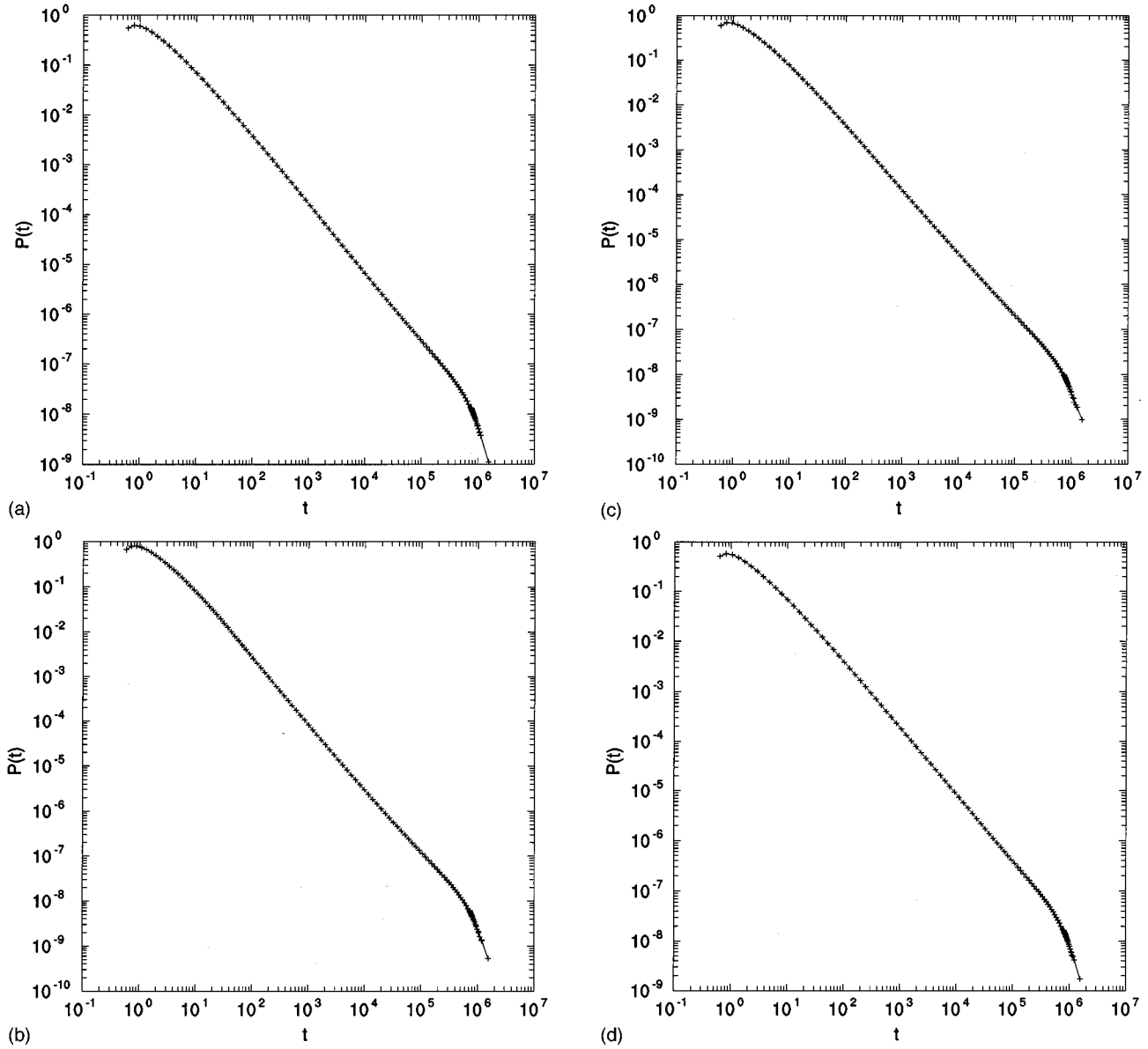

FIG. 5. Transit time distribution for pure convection in five-spot flow for various initial azimuthal angles; $\phi =$ (a) 0, (b) $\pi/12$, (c) $\pi/8$, (d) $\pi/12$.

where $\hat{n}$ is a unit vector of random orientation. The tracer concentration $C(\vec{x},t)$ satisfies $C(\vec{x},t+\Delta t)=C(\vec{x}-\Delta\vec{x},t)$, and if this expression is averaged over realizations of $\hat{n}$ one obtains the CDE in dimensionless form. Although in principle this method is valid at any Péclet number, in practice the statistical fluctuations obscure the result unless $\mathrm{Pe}\gg 1$.

TABLE II. Power-law exponents and exponential decay constants fit to the numerical results for five-spot flow, for various initial azimuthal angles.

ϕ_0	α	$\tau\times 10^{-5}$
0+	1.42 ± 0.02	2.53 ± 0.02
$\pi/12$	1.42 ± 0.02	2.48 ± 0.03
$\pi/8$	1.40 ± 0.03	2.48 ± 0.03
$\pi/6$	1.39 ± 0.03	2.41 ± 0.03
$\pi/4$	1.35 ± 0.05	2.47 ± 0.04

We have applied the single-random-walker method to the three flow fields previously studied in the convective limit. Initially, a random walker is placed at a random position on the surface of a small sphere of radius $r_0=0.01a$ about the source (corresponding to the finite size of a well bore) and then displaced according to rule (18) until the walker reaches the surface of a similar small sphere about the sink. The time step Δt is chosen so that the maximum displacement per step is at most $0.01a$. The Péclet number is defined as $\mathrm{Pe}=au_{\max}/D$, where the maximum velocity $u_{\max}$ is related to the flux Q by $Q=4\pi u_{\max}^2 r_0^2$. The random walk procedure is repeated 500 000 times, and the histogram of arrival times is converted into the probability distribution function $p(t)$ as above. In Fig. 6 we show the results for the simple dipole flow discussed in Sec. II A. At the lowest Pe the curve is noisy and difficult to interpret, but as Pe increases, we see an increasing time interval over which the pure-convection result $p(t)\sim t^{-5/4}$ holds. At long times, noise is still present in

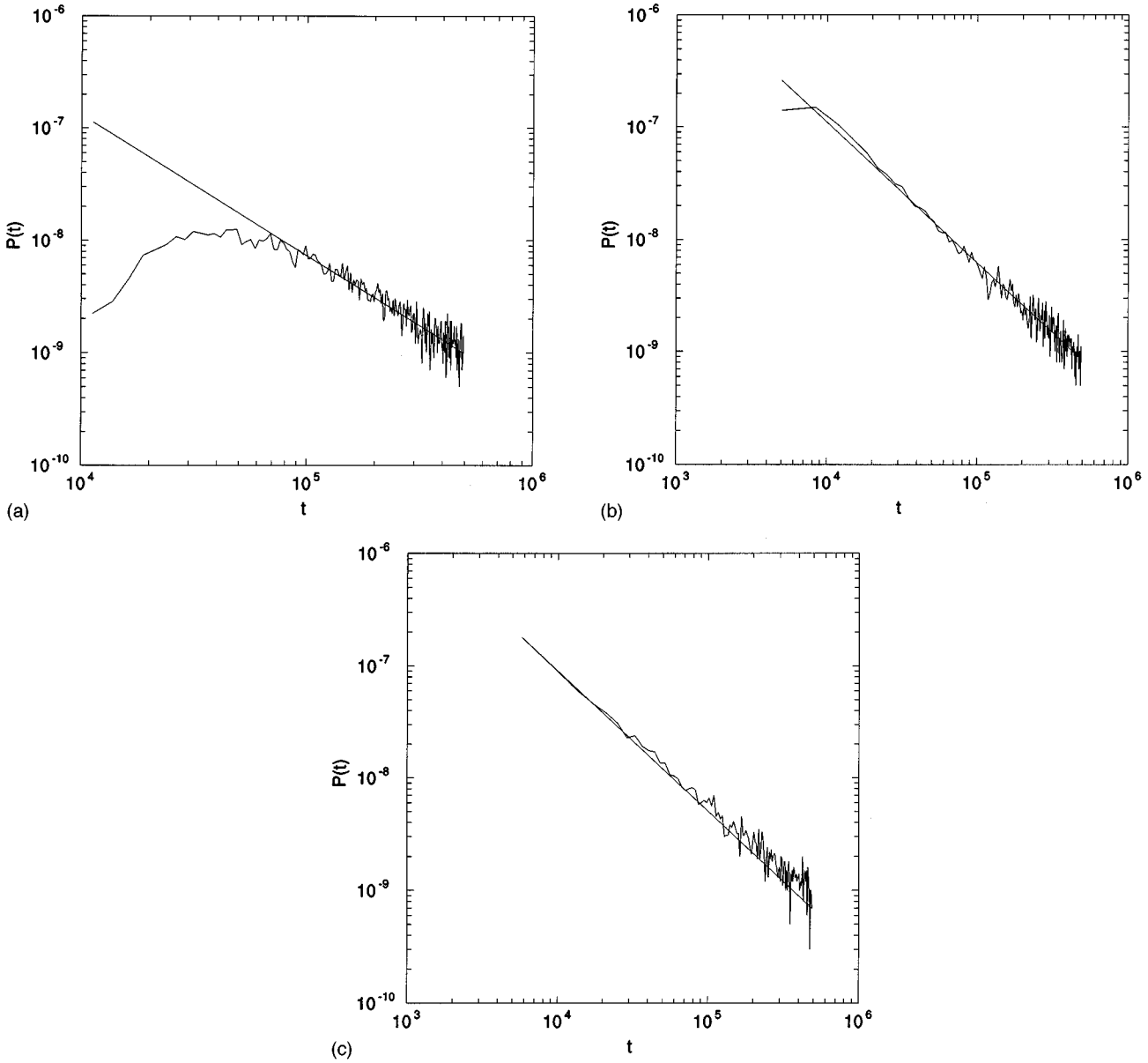

FIG. 6. Single-random-walker calculations of $p(t)$ for a simple dipole flow at various Péclet numbers; (a) Pe=7161, (b) Pe=71 610, and (c) Pe=716 100.

the tail region due to the relatively small number of walkers present there, but there is a hint of the shoulder alluded to in the Introduction. Likewise, for the asymmetric dipole flow [Fig. 7(a)] and the five-spot flow [Fig. 7(b)], at high Pe we observe a region of convective power-law behavior followed by a tail region where statistical fluctuations obscure the result.

The behavior in the tail regions may be computed using methods which rely on the continuum CDE more directly, and in a sense average over the previous fluctuations. As in paper II, we have used two somewhat related methods which might be described as ''probability propagation.'' The simplest procedure is to consider a spatial lattice of spacing ℓ, and let $p(\vec{r},t)$ be the tracer concentration or probability of occupancy of a lattice site $\vec{r}$ at time t. At a later time, this probability hops to nearest neighbor sites according to

$$p(x,y,z,t+\Delta t)=\rho_{x+}p(x-\ell,y,z,t)+\rho_{x-}p(x+\ell,y,z,t)+\rho_{y+}p(x,y-\ell,z,t)+\cdots, \tag{19}$$

where the hopping rates are $\rho_{x\pm}=1/6\pm u_x(\vec{r})\Delta t/2\ell$ and so on, and represent symmetric displacements with a convection-induced bias proportional to the local velocity. In the limit $\Delta t\to 0$, Eq. (19) reproduces the CDE with $D=\ell^2/2\Delta t$. The time step should be chosen small enough that the hopping rates are positive, and a constraint on the maximum value of Pe for a given lattice spacing is thereby implied: $\mathrm{Pe}_{\max}=2a/3\ell$. In Fig. 8 we show results using this method for a representative case: the simple and asymmetric dipole flows at Pe=4.4. A limited range of power-law behavior is present, along with a very prominent shoulder representing the diffusive boundary echoes, previously seen in 2D calculations.

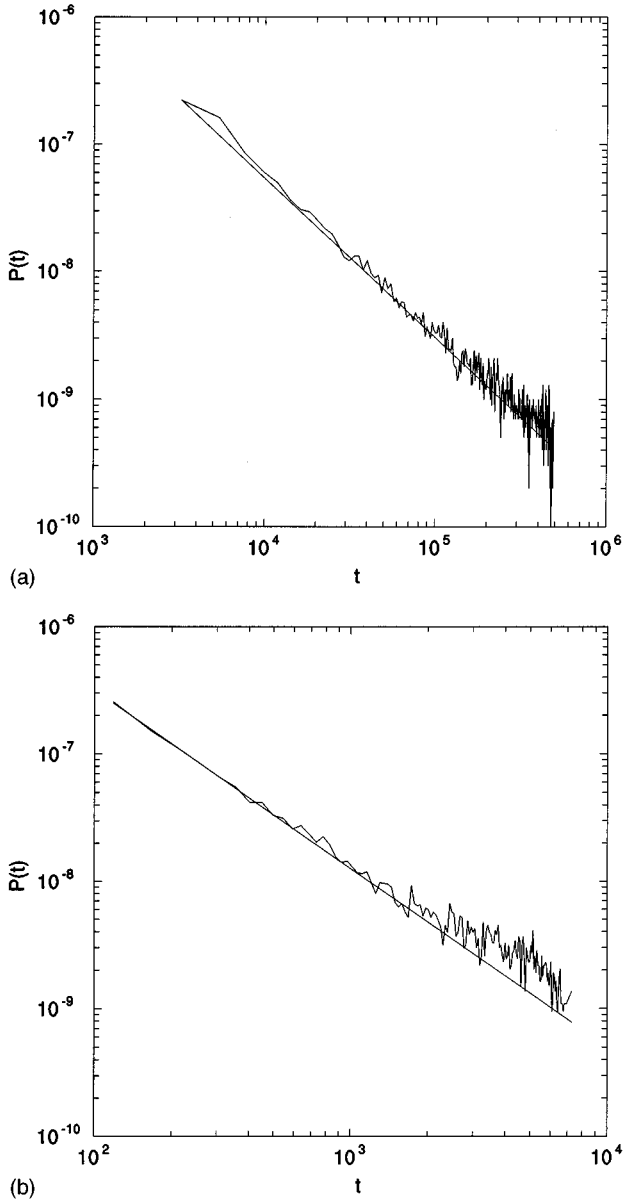

FIG. 7. Single-random-walker calculations of $p(t)$ for (a) asymmetric dipole flow and (b) five-spot flow, both at Pe=716 100.

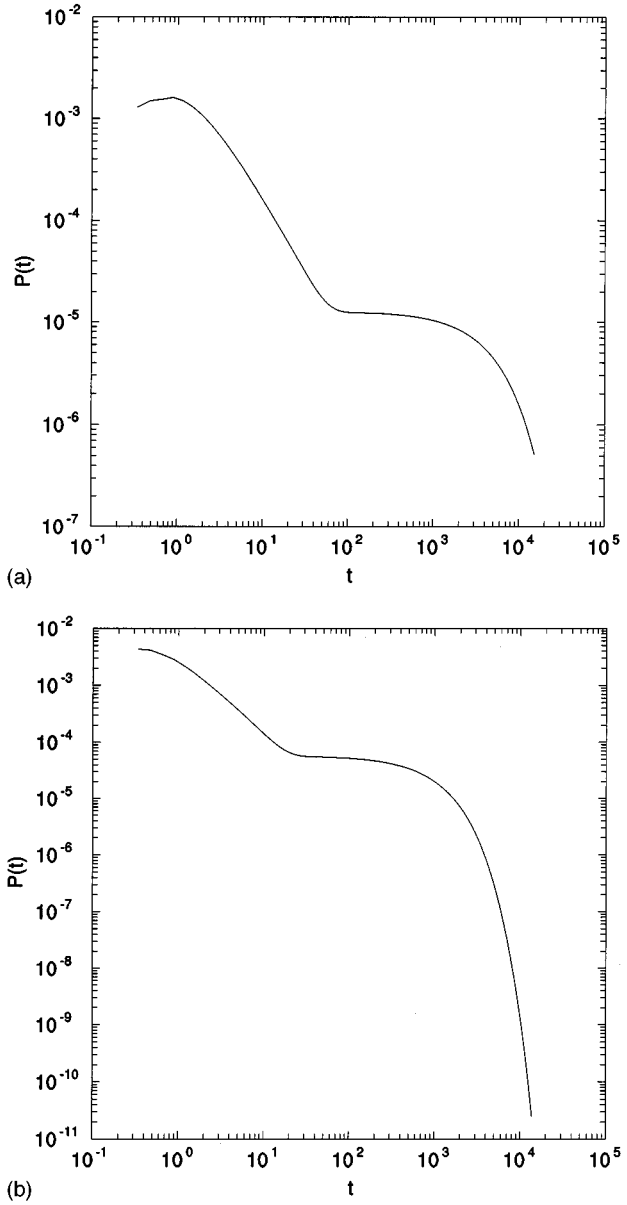

FIG. 8. On-lattice probability propagation results for (a) simple dipole flow and (b) asymmetric dipole flow, both at Pe=4.4.

We have also extended the *off*-lattice continuum method of II to the 3D case. Here one again works with $p(\vec{r},t)$, but the time-evolution rule is to first convect this probability to the position $\vec{r}+\vec{u}(\vec{r})\Delta t$, which is generically not a lattice site. This probability is then redistributed to the adjacent lattice positions in such a way as to conserve the mean position and to relate the mean-square fluctuation to the diffusion coefficient. In detail, suppose the point to which tracer is convected is $\vec{r}=(x,y,z)$ and that the nearest lattice site is the origin, and let w_{ijk} be the fraction of tracer to be distributed to lattice site (i,j,k). We will use the simplest rule, in which w is only nonzero on the six nearest neighbor sites, $(\pm 1,0,0)$, etc. The constraints on w are conservation of tracer,

$$\sum_{ijk} w_{ijk}=1, \tag{20a}$$

no change in mean position,

$$\ell(w_{100}-w_{-100})=x, \text{ etc.}, \tag{20b}$$

and diffusive mean-square displacement,

$$\sum_{ijk} w_{ijk}(x_{ijk}-x)^2=(\Delta x)^2=2D\Delta t, \quad \text{etc.},$$

which translates into

$$(\ell-x)^2 w_{100}+x^2(w_{010}+w_{0-10}+w_{001}+w_{00-1}+w_{000})$$
$$+(\ell+x)^2 w_{-100}=2D\Delta t, \tag{20c}$$

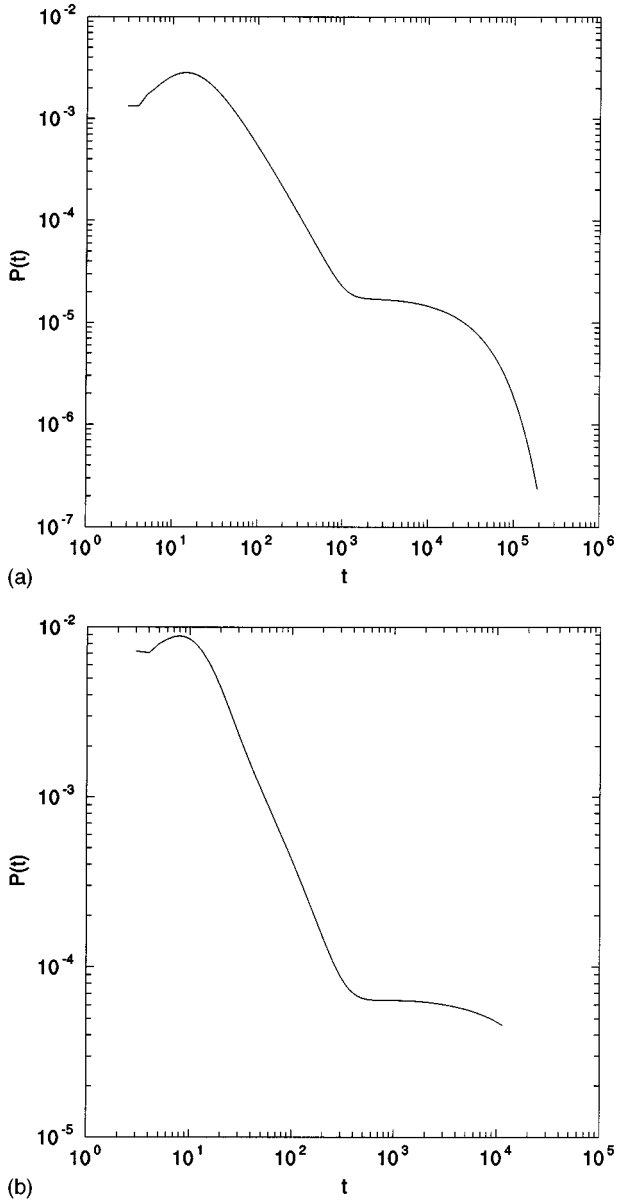

FIG. 9. Off-lattice probability propagation results for (a) simple dipole flow and (b) five-spot flow, both at Pe=4.4.

etc. The solution of these equations is

$$w_{000}=1-\frac{x^2+y^2+z^2+6D\Delta t}{2\ell^2},$$

$$w_{\pm 100}=\frac{2D\Delta t\pm x(\ell\pm x)}{2\ell^2}, \quad \text{etc.} \tag{21}$$

Again as in II, there are constraints which follow from positivity of the redistribution probabilities. If we define $d=2D\Delta t/\ell^2$, then $w_{000}>0$ gives an upper bound on d, while $w_{100}>0$ gives a lower bound. Ostensibly we can have $\vec{r}^2=3\ell^2/4$, since the origin is the nearest lattice site to $\vec{r}$, but in this case no value of d ensures positive w's. We avoid the difficulty by limiting the convective steps to $|x|,|y|,|z|\leq\ell/3$, in which case $d=2/9$ is satisfactory. There is a resulting maximum Péclet number of $3\sqrt{3}a/\ell$. We illustrate the method in Fig. 9, where we have considered the simple dipole and five-spot flows at Pe=4.4. The simple dipole results are consistent with the earlier probability propagation method, and in both cases we again see a power-law interval with the convective exponent and a diffusive shoulder.

IV. EFFECTS OF HETEROGENEITY

Up to now, we have considered porous media that are statistically homogeneous and isotopic, so that the continuum equations used above have constant coefficients. Realistically, petroleum reservoirs and aquifers have property variations on a range of length scales ranging from the pore scale fluctuations which have been implicitly averaged over here to macroscopic geological features [13]. It is therefore appropriate to investigate the effect of such heterogeneities on the characterization of the transit time distribution proposed here. The range of possibilities is too great for a systematic survey, so we will consider three cases—uncorrelated fluctuations in the velocity field, layered but otherwise uncorrelated fluctuations (representing the effects of geological stratification), and an example of a macroscopic barrier.

A. Uncorrelated fluctuations

We begin with the case of a quenched random fluctuation in the velocity field, taken in the form

$$\vec{u}(\vec{x})=\vec{u}_0(\vec{x})+\vec{u}_r(\vec{x})+\vec{u}_c(\vec{x}). \tag{22}$$

In this expression, $\vec{u}_0$ is the unperturbed source-sink velocity field, and the random perturbation is $\vec{u}_r(\vec{x})=\lambda\ \xi(\vec{x})\vec{u}_0(\vec{x})$, where λ is an adjustable magnitude, and ξ is a random number in the interval $[-1,1]$ assigned at each lattice point. While $\vec{u}_0$ is an incompressible velocity field by construction, the uncorrelated random term has a nonzero divergence in general. We restore incompressibility by adding a counterterm $\vec{u}_c\equiv\vec{\nabla}\Phi_c$, where $\nabla^2\Phi_c=-\vec{\nabla}\cdot\vec{u}_r$. The Poisson equation for Φ_c is solved numerically using a standard solver [14] and differentiated numerically to obtain $\vec{u}_c$. The tracer motion is obtained using the single-random-walker method; fluctuations in the velocity would be most significant at high Pe, so we restrict ourselves to this regime. Since the tracer motion in this method is not restricted to the lattice sites where $\vec{u}_r$ and $\vec{u}_c$ are defined, the values of the latter two fields are obtained by numerical interpolation.

In Fig. 10 we show $p(t)$ for three choices of fluctuation strength $\lambda=0.01$, 0.1, and 0.5, for a simple dipole flow in a sphere of radius $R=30$. (We use a smaller system than previously, due to the computational cost associated with solving the Poisson equation, and the time interval where power-law behavior applies is correspondingly reduced.) The trend of the results is that for small enough λ the results are indistinguishable from simple dipole flow, for intermediate values the transit time distribution is noticeably altered but the $t^{-5/4}$

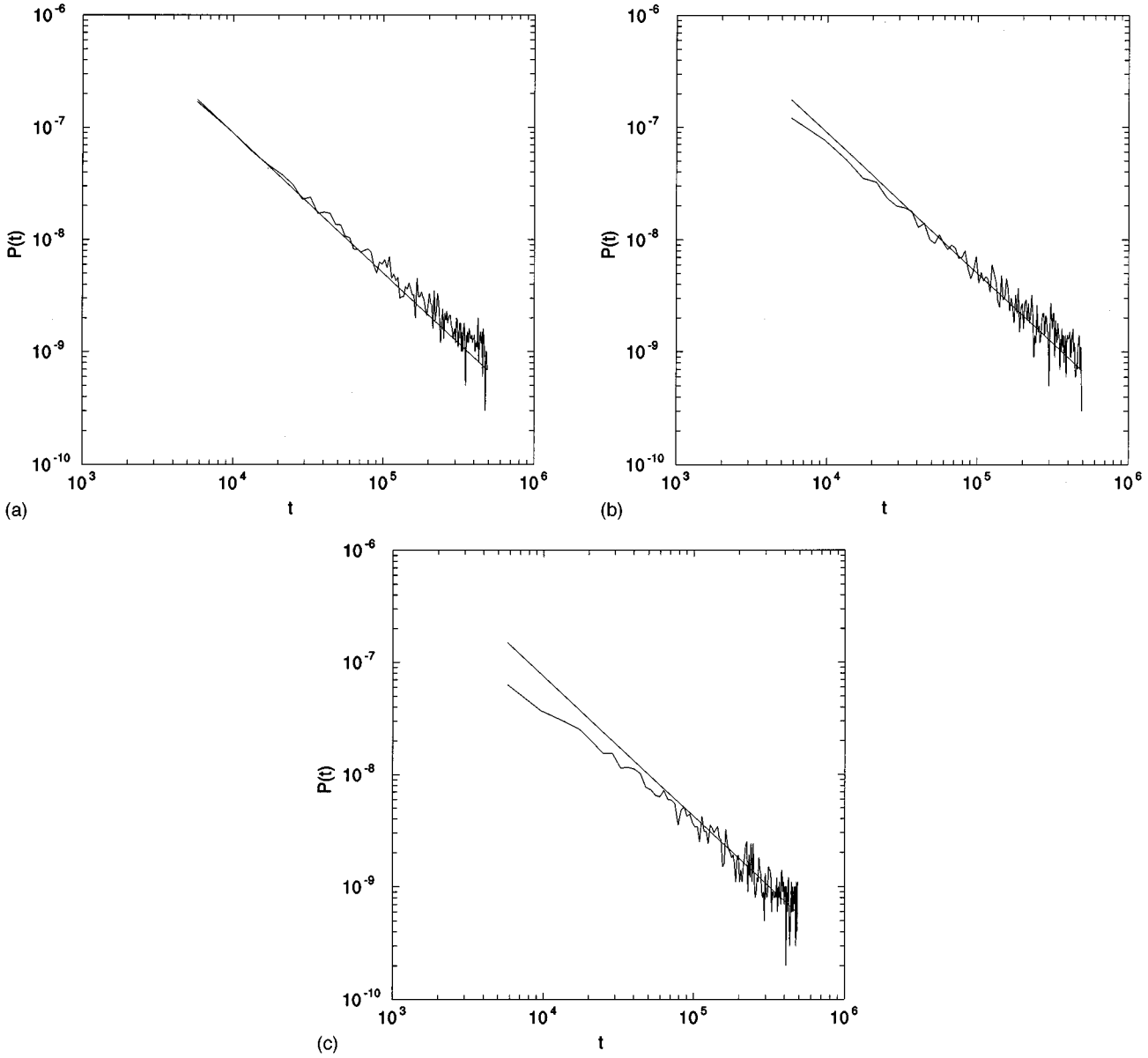

FIG. 10. Effects of uncorrelated fluctuations on $p(t)$: simple dipole flow at Pe=716 100 using the single-random-walker method for various fluctuation strengths. $\lambda =$ (a) 0.01, (b) 0.1, (c) 0.5.

power law is still recognizable, but for $O(1)$ fluctuations it is difficult to recognize a power law at all. The behavior of $p(t)$ correlates with the alteration in typical individual particle trajectories, illustrated in Fig. 11. Realistic geological systems often show prominent stratification [13], and we have considered one example, where we suppose that layers are oriented parallel to the x-y plane. In Eq. (22), we then take $\lambda \rightarrow \lambda(z)$ with layers of thickness 5 and $\lambda(z)$ piecewise constant within each, with values chosen randomly between 0 and 0.5. The power-law behavior is still evident. The conclusion from this set of examples is that the predicted power-law behavior in Eq. (14) is robust, and will survive under perturbations which are not too strong. We have also considered the transit time distribution at lower Pe in the presence of fluctuations using the probability propagation method, and even for $\lambda = 0.5$ there is only a slight change in the computed $p(t)$, and the shoulder in particular.

B. Effects of an impermeable barrier

If we introduce a major change in the flow pattern, we expect that the global shape of the streamlines is altered and, in the light of the results of paper II and the analytic estimates in Sec. II B, a change in exponent. We illustrate this behavior by the single example of a large impermeable barrier placed in the simulated reservoir. We consider a cubic geometry of $-L<x,y,z<+L$, with a source-sink pair at $(0,0,\mp a)$ with a barrier in the region behind the source: $\{-L<x<0, -L<y<L, -2a<z<-3a\}$. The streamlines in the meridional $(y=0)$ plane are shown in Fig. 12, where we have adopted the values $L=8$ and $a=1$, and were obtained from a numerical solution of the Poisson equation for the velocity potential, with Neumann boundary conditions on the sides of the cube and the barrier. The tracer transit time distribution was studied for various ranges of Pe using all of the methods described above.

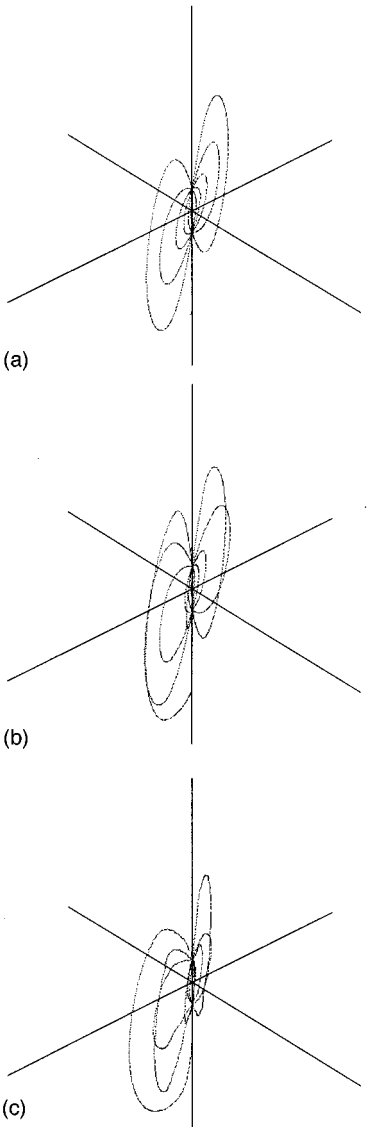

FIG. 11. Typical particle trajectories in the velocity fields corresponding to Fig. 10.

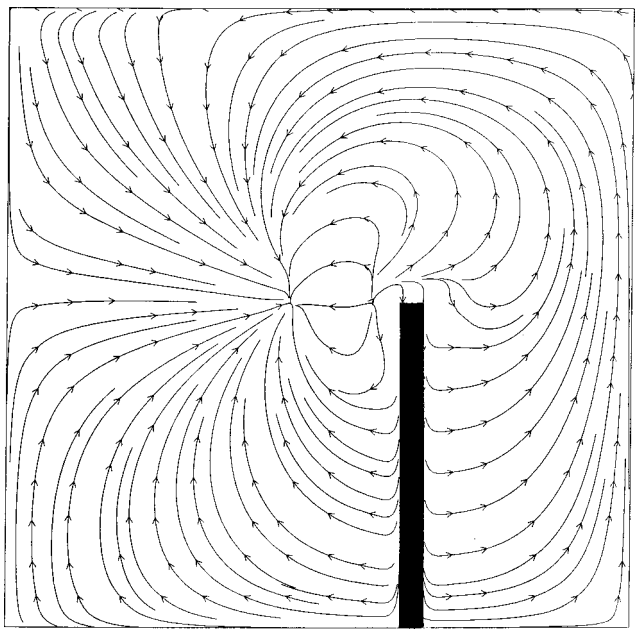

FIG. 12. Streamlines in the $y=0$ plane for the barrier example of Sec. IV B.

For pure convection, there is a clear distinction between trajectories emitted in the two half spaces away from or towards the barrier. For the former group, $x_0>0$ or $\phi_0<|\pi/2|$, the meridional streamlines at least are qualitatively similar to those of simple dipole flow, and indeed as seen in Fig. 13(a) the simple dipole exponent $p(t)\sim t^{-5/4}$ applies. The second group consists of trajectories emitted into the lower half plane, and now the behavior is sensitive to the initial value of θ. Here, Fig. 12 suggests that if θ_0 is not too close to π the streamlines are again roughly dipolar, but otherwise they are substantially altered. Since increasing θ increases the transit time, we would expect $p(t)$ to have a dipolar $t^{-5/4}$ regime at moderate times, crossing over to some other behavior at longer t. The result of the convective calculation shown in Fig. 13(b) for $\pi/2<|\phi_0|<\pi$ confirms this prediction; there is a dipolar interval at short times, crossing over to $t^{-1.39}$, and eventually an exponential decay due to finite system size. In two dimensions (paper II) we could use conformal mapping methods to argue analytically that the presence of a large barrier would produce a power-law decay with exponent 6/5, independent of the details of shape. Here only numerical methods are available, and we can only conjecture that the barrier exponent is universally approximately 1.39.

Next we consider the effects of diffusion. In Fig. 14, we show the results of single-random-walker simulations for $\mathrm{Pe}=4.8\times10^6$, again dividing the walker into two groups where the initial orientation is away from or towards the barrier. As in the cases discussed in Sec. III, diffusion adds fluctuations to $p(t)$ which grow as time increases, but the power-law decay regimes are still clearly identifiable. At low Pe, the behavior is somewhat different. Figure 15(a) shows the transit time distribution in the cube without the barrier present, at $\mathrm{Pe}=10$. The power-law regime and diffusive shoulder are present, as in the sphere examples of Sec. III, and verify that the behavior we are discussing is not sensitive to the overall shape of the flow region provided it is ''rounded.'' With the barrier present, Fig. 15(b), there are deviations from straight-line behavior at short times, and a more rapid decay at longer times, the latter due to the system being effectively smaller. At still lower $\mathrm{Pe}=1.5$, shown in Fig. 15(c), the power-law region is simply absent.

V. CONCLUSIONS

We have examined some of the generic properties of the hydrodynamic dispersion of a passive tracer in ''reservoir'' situations, where the background fluid flow occurs between localized sources and sinks in a finite-sized three-dimensional porous medium. The quantity of greatest interest is the transit time probability distribution $p(t)$, which may be measured by examining the tracer concentration outside the reservoir itself. As in the two-dimensional cases con-

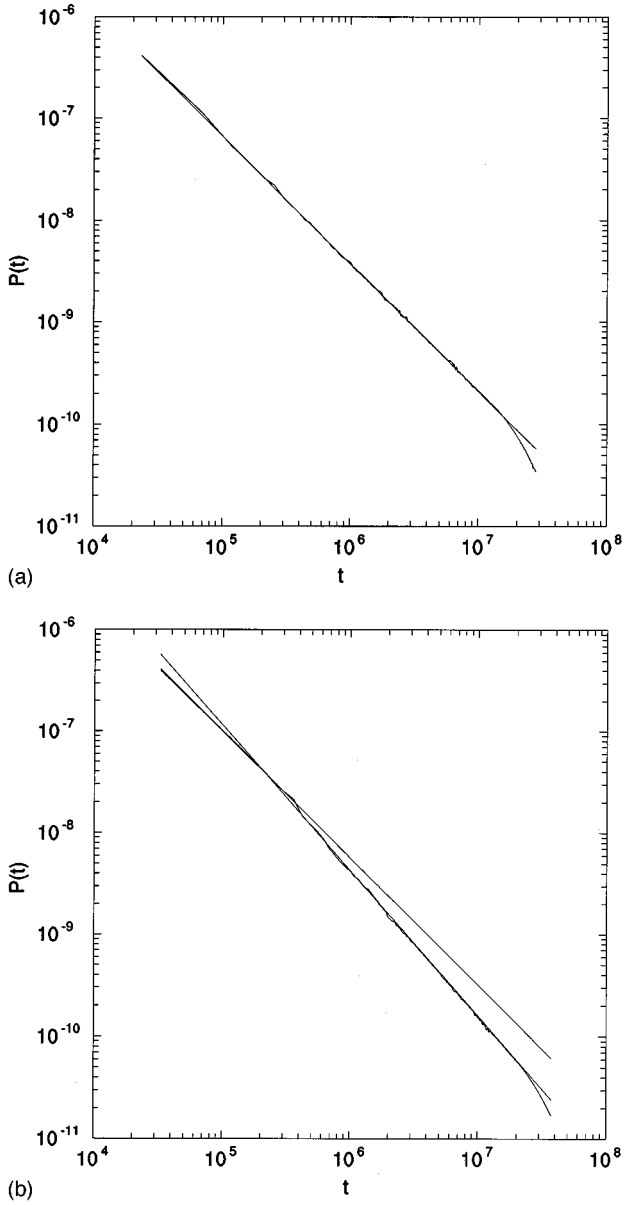

FIG. 13. Behavior of the transit time distribution in the pure convection limit for the barrier example. (a) Tracer emitted away from the barrier, and (b) tracer emitted towards the barrier.

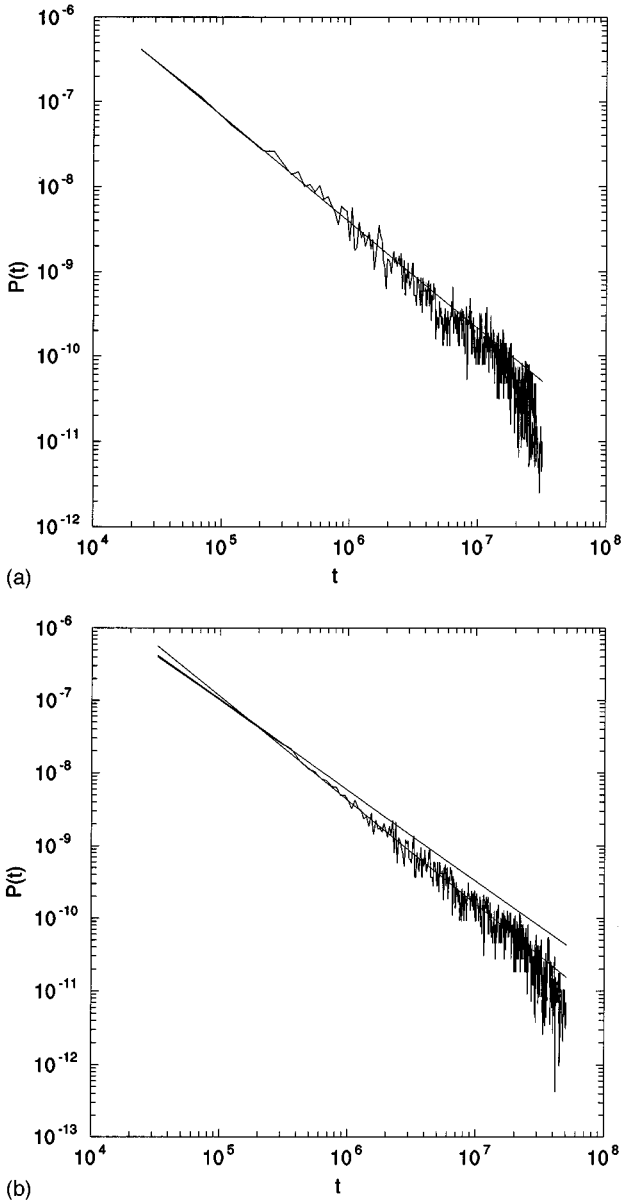

FIG. 14. Single-random-walker simulations of $p(t)$ for the barrier example at high Pe, in the same format as Fig. 13.

sidered previously by us, and in contrast to the well-studied case of quasi-one-dimensional flows, $p(t)$ displays regions of power-law and exponential decay separated by a shoulder, and the parameters of these features may be precisely correlated with the geometry and flow field within the reservoir. The power-law exponent can be related to the multipole order of the source-sink distribution by an algebraic relationship, the location of the shoulder is connected via diffusion to the size of the reservoir, and the exponential decay constant can be related to the velocity field near stagnation points in the flow. The results are not sensitive to the presence of ''weak'' disorder, meaning uncorrelated local perturbations which are not too strong, but under $O(1)$ perturbations in highly heterogeneous systems one can see different behavior. The qualitative distinction between the two cases is just that weak perturbations do not alter the global shape of the streamlines.

The behavior discussed in this paper indicates that simple noninvasive measurements of dispersion in porous media flows contain extensive information about the geometry of the flow domain. The key ingredient is the kinematics of convective motion on fluid streamlines, and the methods developed here may be applicable to other situations where hydrodynamic dispersion enters. In terms of general knowledge, we have shown that even relatively simple flow configurations display a variety of scaling laws and surprising connections between flow and tracer motion. A modest application of these results is to provide a check on any more detailed calculation by elucidating some generic features of the transit time distribution. More importantly, in practical situations involving underground reservoirs where one has

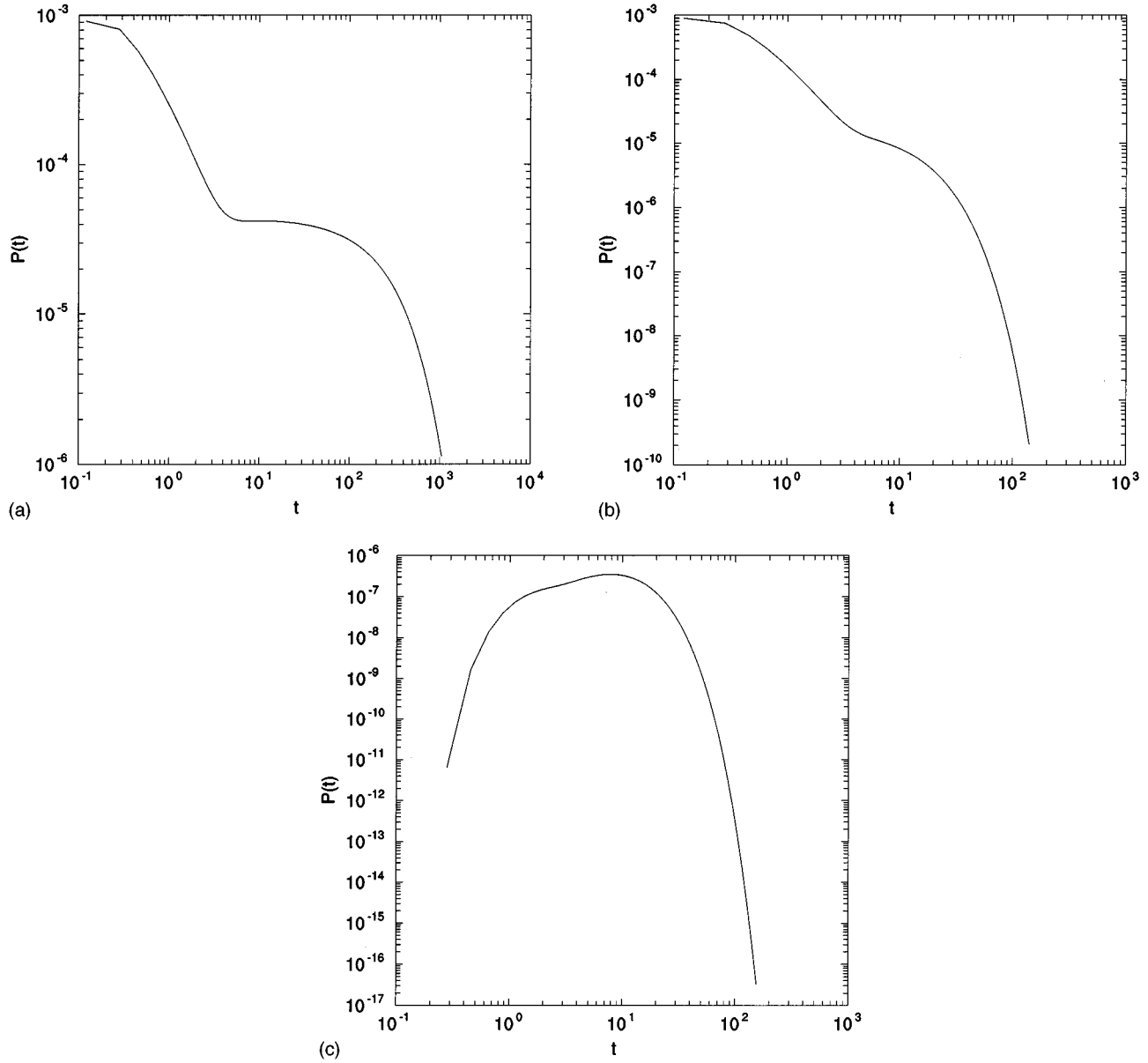

FIG. 15. Effects of the barrier on the transit time distribution at low Pe, using the probability propagation method. (a) $p(t)$ at Pe$=10$ in a cube of side $2L$, *without* the barrier, (b) the same, *with* the barrier present, (c) Pe$=1.5$, with the barrier.

only limited subsurface information, the results of this work allow one to partially characterize the geometry by standard field measurements alone.

ACKNOWLEDGMENTS

We have benefited from discussions with E. J. Hinch, J. P. Hulin, and S. Redner. This research was supported by the Office of Basic Energy Sciences of the U.S. Department of Energy.

APPENDIX

The exponents for power-law decay of $p(t)$ in any dimensionality are given by the following dimensional analysis argument, due to Hinch [10]. For an nth-order multipole in d dimensions, the velocity potential is

$$\Phi(\vec{r})=Af(\vec{\Omega})r^{2-n-d},$$

where $\vec{\Omega}$ refers to the $d-1$ angular variables, and the power of r follows from the fact that a monopole ($n=0$) satisfies $\nabla^2\Phi=\delta^d(\vec{r})$. The relation between velocity and potential, $\vec{u}=\vec{\nabla}\Phi$, gives the dimensions $[\Phi]=L^2/T$, where L and T are length and time scales, so that $[A]=L^{n+d}/T$. Now let $\Psi(t)$ be the flux of tracer particles leaving a small sphere about the source which arrive at the sink at times greater than t. (The stream function in 2D has a somewhat similar interpretation, hence the notation.) Since flux has the dimensions

of velocity times [$(d-1)$-dimensional] area, $[\Psi]=L^d/T$, and since the only dimensionful quantities on which $\Psi(t)$ can depend are A and t itself,

$$\Psi(t)=\alpha A^{d/(n+d)}t^{-n/(n+d)},$$

where α is a pure number. The rate at which tracer particles arrive at the sink is then

$$p(t)\sim-\Psi'(t)\sim t^{-(2n+d)/(n+d)}, \tag{A1}$$

in agreement with the results in this paper and II. Note that the exponent is always between -1 and -2, in accord with the general constraints noted in II.

[1] J. Bear, *Dynamics of Fluids in Porous Media* (Elsevier, Amsterdam, 1971).

[2] A. E. Scheidegger, *The Physics of Flow in Porous Media*, 3rd ed. (University of Toronto Press, Toronto, 1974).

[3] F. A. L. Dullien, *Porous Media: Structure and Fluid Transport*, 2nd ed. (Academic, London, 1991).

[4] M. Sahimi, Rev. Mod. Phys. **65**, 1393 (1993).

[5] *Disorder and Mixing*, edited by E. Guyon, J.-P. Nadal, and Y. Pomeau (Kluwer, Dordrecht, 1988).

[6] P. Kurowski, I. Ippolito, J. P. Hulin, J. Koplik, and E. J. Hinch, Phys. Fluids **6**, 108 (1994).

[7] J. Koplik, S. Redner, and E. J. Hinch, Phys. Rev. E **50**, 4650 (1994).

[8] J. Koplik, S. Redner, and E. J. Hinch, Phys. Rev. Lett. **74**, 82 (1995). Some of the results of this paper were obtained independently by L. Mittag and M. J. Stephen, J. Stat. Phys. **78**, 377 (1995).

[9] J. D. Jackson, *Classical Electrodynamics*, 2nd ed. (Wiley, New York, 1975).

[10] E. J. Hinch (private communication).

[11] M. Zhang, Ph.D. thesis, City University of New York, 1996.

[12] C. W. Gardiner, *Handbook of Stochastic Methods*, 2nd ed. (Springer, New York, 1985).

[13] *Reservoir Characterization*, edited by L. W. Lake and H. B. Carroll (Academic, New York, 1986).

[14] D. C. Kahaner, C. Moler, and S. Nash, *Numerical Methods and Software* (Prentice-Hall, Englewood Cliffs, NJ, 1989).